Microhardness and friction coefficient of multi-walled carbon nanotube-yttria-stabilized ZrO_2 composites prepared by spark plasma sintering

A. Kasperski, A. Weibel,* D. Alkattan, C. Estournès, V. Turq, Ch. Laurent and A. Peigney

Université de Toulouse, Institut Carnot CIRIMAT, UPS CNRS, Université Paul-Sabatier, 31062 Toulouse Cedex 9, France

Multi-walled carbon nanotubes (eight walls) are mixed with an yttria-stabilized ZrO_2 powder. The specimens are densified by spark plasma sintering. Compared to ZrO_2, there is a 3.8-fold decrease of the friction coefficient against alumina upon the increase in carbon content. Examinations of the friction tracks show that wear is very low when the carbon content is sufficient. Exfoliation of the nanotubes due to shearing stresses and incorporation of the debris into a lubricating film over the contact area is probable.

Keywords: Spark plasma sintering; Carbon nanotubes; Zirconia; Friction

Carbon-containing composites, notably in the form of carbon nanotubes (CNTs), are of particular interest for tribological applications. Reports on CNT–metal [1,2] and CNT–Al_2O_3 composites [3–7] are increasingly abundant. The homogeneity of the CNT dispersion, good interfacial bonding and a high relative density are key points to achieving higher microhardness, lower friction and lower wear. However, the comparison of the results reported by different groups is hampered, notably because different types of CNTs or even carbon nanofibers (CNFs) are used, the preparation routes differ markedly, and the tribological testing conditions (counterface, load, distance, relative humidity) vary widely. The aim of this work is to prepare multi-walled CNT (MWCNT)-yttria-stabilized ZrO_2 composites, the tribological properties of which have not been reported to the best of our knowledge, and investigate the friction against alumina. The results are compared to those obtained using single-wall CNTs (SWCNTs) [8] and CNFs [9].

A commercial 3 mol.% yttria-stabilized zirconia powder (TZ-3Y, Tosoh, Japan) was used for the study. The proportions of tetragonal and monoclinic ZrO_2 are 77 and 33 vol.%, respectively. The average grain size is slightly less than 100 nm. MWCNTs were purchased from Nanocyl (Belgium). The average number of walls (eight walls) and average outer diameter (10.2 nm) were determined from the measurement of about 100 CNTs on high-resolution transmission electron microscopy (HRTEM) images obtained using a JEOL JEM 2100F [2]. The MWCNTs were dispersed in nitric acid (3 mol L^{-1}) using 1 mL of nitric acid per mg of CNTs and reflux overnight (magnetic stirring, 130 °C). The suspension was neutralized and filtered. Raw and acid-treated MWCNTs were characterized by Raman spectroscopy (Jobin-Yvon LabRAM HR800, laser excitation at 632.82 nm). The ratio between the intensities of the D band and the G band (I_D/I_G) in the high-frequency range of the Raman spectra (not shown) is similar after acid treatment (1.80 vs. 1.86), revealing no damage to the MWCNTs. The appropriate amount of acid-treated CNTs, calculated using the CNT density chart [10], was dispersed in deionized water with a sonotrode for 15 min. The CNT suspension was poured into a suspension of zirconia in water (pH 12) that had been prepared previously (15 min sonication and 1 h mechanical stirring). The mixture was sonicated for 30 min. The vessel containing the MWCNT–ZrO_2 suspension was immersed in liquid N_2 until freezing and freeze-dried (Christ alpha 2–4 LD, Bioblock Scientific) at −84 °C for 48 h in a primary vacuum (12 Pa). The carbon content (C_n) in the thus-obtained MWCNT–ZrO_2

* Corresponding author. Tel.: +33 0561556175; fax: +33 0561556163.; e-mail: weibel@chimie.ups-tlse.fr

http://dx.doi.org/10.1016/j.scriptamat.2013.05.015

composite powders is equal to 0.55, 1.00, 1.68, 3.24 and 5.16 wt.%. For all composite powders, $I_D/I_G = 1.86 \pm 0.12$, showing that the mixing process did not induce damage to the MWCNTs.

The ZrO_2 and MWCNT–ZrO_2 powders were densified by spark plasma sintering (SPS, Dr. Sinter 2080, SPS Syntex Inc., Japan). Into a 20 mm inner diameter graphite die were loaded, from bottom to top, a graphite punch, a sheet of graphitic paper, an alumina powder bed about 1.2 mm thick (in order to block the current and ensure a similar heating in specimens with different electrical conductivities), a sheet of graphitic paper, the powder sample, then the same materials in reverse order. Graphitic paper was also placed along the die for easy removal. SPS was performed in argon. A pulse pattern of 12 current pulses followed by two periods of zero current was used. A heating rate of 250 °C min^{-1} was used from room temperature to 600 °C, where a hold of 3 min was applied in order to stabilize the temperature reading. Then, a heating rate of 100 °C min^{-1} was used from 600 to the dwell temperature, either 1200, 1250 or 1300 °C according to the increasing carbon content (Table 1), where a 10 min dwell was applied. A uniaxial charge (corresponding to 100 MPa on the pellet) was gradually applied during the hold at 600 °C and maintained during the remaining heating and the dwell. It was released within the last minute of the dwell. The cooling rate was equal to 60 °C min^{-1}. The sintered specimens were in form of pellets 20 mm in diameter and about 2 mm thick. The pellets were polished down to 1 μm using diamond slurries. The sintered specimens will be denoted ZrO_2, S0.5, S1, …, S5 hereafter.

Analysis of the X-ray diffraction (XRD, Bruker D4 Endeavor) patterns (not shown) revealed only the presence of tetragonal zirconia. The density of the pellets was determined by the Archimedes method after removal of the graphitic surface contamination layer by light polishing. The relative densities (Table 1), calculated using 6.05 g cm^{-3} for tetragonal zirconia and 1.83 g cm^{-3} for MWCNTs, are in the range 98–100% for ZrO_2, S0.5, S1 and S2 and decrease for higher carbon contents, reaching 94% for S5, reflecting that increasing CNT content inhibits densification [11]. For all densified composites, $I_D/I_G = 1.84 \pm 0.14$, indicating that the MWCNTs were not grossly damaged by SPS.

Field emission gun-scanning electron microscopy (FESEM, JEOL JSM 6700F) observations of the fracture surface of the ZrO_2 sample (Fig. 1a) reveal that the grain size is equal to 100 ± 10 nm, only slightly higher than in the starting powder. The same size is observed for the zirconia matrix in all composites. For S2 and S5, increasing amounts of MWCNTs well distributed along the grain boundaries of the matrix (Fig. 1b and c) hampered grain growth despite the higher sintering temperature for S5, thus accounting for the lower relative density.

Table 1. Carbon content by weight (C_w), SPS dwell temperature (T_{SPS}), relative density (d), Vickers microhardness (H_V), average arithmetic roughness (R_a), average friction coefficient against an alumina ball for a 5 N load (μ_5) and a 10 N load (μ_{10}).

Specimen	C_n (wt.%)	T_{SPS} (°C)	d (%)	H_V (GPa)	R_a (μm)	μ_5	μ_{10}
ZrO_2	0	1200	98	14.5	0.01	0.57	0.54
S0.5	0.55	1200	100	13.7	–	0.57	0.61
S1	1.00	1200	99	12.9	–	0.61	0.55
S2	1.68	1200	98	11.4	0.03	0.47	0.48
S3	3.24	1250	97	10.1	0.02	0.35	0.34
S5	5.16	1300	94	10.1	0.11	0.15	0.14

The indentation tests (3 N applied for 10 s in air at room temperature) were performed on the polished surface of the specimens by loading with a Vickers indenter (Shimadzu HMV 2000). The calculated microhardness values (H_V, Table 1) are the average of 10 measurements. The Vickers microhardness for the ZrO_2 specimen is equal to 14.5 GPa; it decreases smoothly with the increase in carbon content, reaching 10.1 GPa for S3 and S5. These values are higher than those reported for MWCNT–ZrO_2 [12,13] and CNF–ZrO_2 composites [14,15] for which composite powders were also prepared by a mixing route. The higher values obtained in this study could reflect a better dispersion of CNTs in the matrix and/or a slightly lower matrix grain size.

Friction tests were performed using a pin-on-disc reciprocating flat geometry (CSM Tribometer) in ambient air (30–60% relative humidity, room temperature). An alumina ball 6 mm in diameter was used against flat ZrO_2 and CNT–ZrO_2 sample surfaces. The sliding speed was fixed at 5 cm s^{-1}. The tests were performed at 5 and 10 N normal load. Higher loads were not tested in order to avoid damaging the pellets and changing the contact geometry. The frictional force transferred to a load cell was recorded throughout the test. Typical curves showing the friction coefficient against the alumina ball vs. distance, for a 5 N load, are shown in Figure 2a. The behavior at 10 N is similar. After a running-in period, the friction coefficient (μ_5 and μ_{10} for a 5 and 10 N load, respectively) is stabilized and the average value on the last 5 m of the test is reported in Table 1 and Figure 2b. For S0.5 and S1, μ increases sharply during the running-in period, at a lower sliding distance than it does for ZrO_2, and stabilizes at a value equal to or slightly higher than the one found for ZrO_2 ($\mu_5 = 0.57$). Thus, small amounts of CNT probably weaken the zirconia grain boundaries but do not provide a lubricating effect, in agreement with results on SWCNT–ZrO_2 composites [8]. For S2 and S3, the evolution of μ is similar to that found for ZrO_2, but with a lower amplitude. The behavior for S5 is markedly different: after the initial increase during running-in (a sliding distance of only 0.7 m), μ decreases smoothly, with a much less noisy curve, down to $\mu_5 = 0.15$, i.e. 3.8 times lower than for ZrO_2. Thus lower densification for S5 is not detrimental, in agreement with results obtained for CNT–Al_2O_3 composites [4]. This could indicate that S5 suffers only mild wear, because the observed noise usually reflects that the contact lacks stability and a certain amount of wear.

The friction tracks made on the specimens using a 10 N load were observed by white-light interferometry optical imaging (Fig. 3). The average arithmetic roughness (R_a, Table 1) is similar for ZrO_2, S2 and S3 (in the range 0.01–0.03) but is significantly higher (0.11) for S5. This could reflect an easier pulling-out of ZrO_2 grains during polishing for S5. The width and depth of the friction tracks increase with the increase in carbon content, reaching a maximum for S3, which could reflect

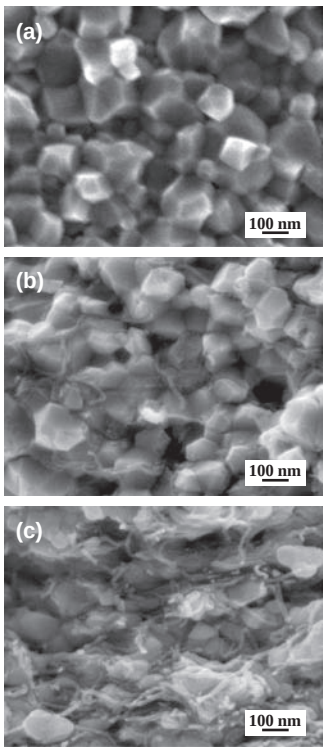

Figure 1. FESEM images of the fracture surface of ZrO_2 (a), S2 (b) and S5 (c).

the corresponding decrease in microhardness (Table 1). However, the track is much fainter for S5 despite the lower relative density and same microhardness than S3, which could reflect a significantly higher wear resistance for S5. The evolution of the worn surface on the alumina ball (not shown) is similar. Carbon debris were observed both on the ball and on the specimen for all composites tested, but the amount is much lower for S5, which is in line with the less noisy friction curve and fainter wear track.

FESEM images of the friction tracks on ZrO_2 (Fig. 4a) reveal numerous cracks roughly perpendicular to the friction direction as reported by other authors [8]. Lateral cracks and also surface cracks and pulled-out grains are observed for S0.5, S1 and S2, but debris are observed on both sides of the track and notably at its end where it spreads, forming a kind of film (Fig. 4b). The back-scattered electron image in compositional mode (Fig. 4c) shows that the film seems to be made up of carbon debris probably mixed with the smaller of zirconia and alumina wear products, the larger ones being projected on the sides and at the end of the track. For S3 (Fig. 4d) and S5, this film is more compact and continuous along the track, which is in line with the lower friction coefficient and less noisy curves. The film is probably richer in carbon for S5, which could account for the higher lubricating effect. Such smearing of carbon-based transferred films over the contact area, which permits easy shear and helps to achieve a lubricating effect during sliding, was reported for CNF–ZrO_2 composites (CNF diameter 80–150 nm, 1.07 wt.% of C, $H_v = 8.1$ GPa and d = 90%) which showed a lower friction coefficient against alumina (5 N load) compared to ZrO_2 (0.35 vs. 0.50) but similar wear [9].

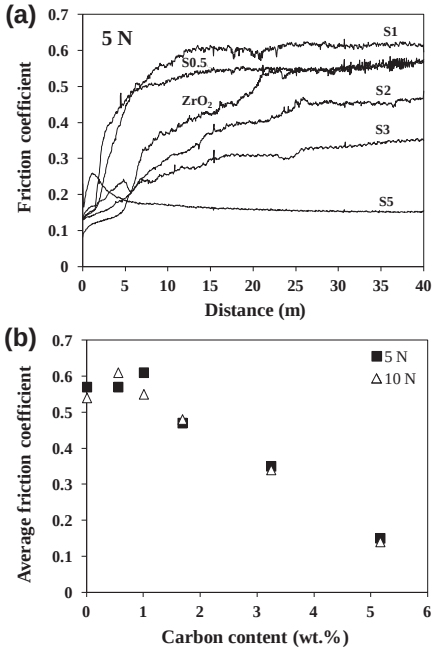

Figure 2. Friction coefficient against an alumina ball vs. the distance for a 5 N load (a) and average friction coefficient vs. carbon content (b). The test load is indicated.

No MWCNTs were identified in the tracks on the FESEM images, either because the film is too compact or because they were exfoliated (i.e. destroyed) owing to shear stresses during the test. The minimum shear strength reached at the sample surface during the present friction tests is calculated using Eq. (1):

$$\tau\,(\mathrm{MPa}) = F_f/A = \mu F/A \quad (1)$$

where F_f is the tangential shearing force (N), μ is the friction coefficient, F is the applied force (N) and A is the contact surface area (mm^2) calculated for a ball/plane contact using Eqs. (2)–(4):

$$a = (3FR^*/2E^*)^{1/3} \quad (2)$$

where a is the contact surface radius, R^* is the equivalent contact radius and E^* is the equivalent Young's modulus, defined as follows:

$$R^* = R/2 \text{ (ball –plane contact)} \quad (3)$$

$$1/E^* = (1 - \nu_{ball}^2)/E_{ball} + (1 - \nu_{plane}^2)/E_{plane} \quad (4)$$

where E and ν are the Young's modulus and the Poisson coefficient, respectively, of the counterparts ($E_{alumina} = 390$ GPa, $\nu_{alumina} = 0.27$, $E_{sample} = 212$ GPa, $\nu_{sample} = 0.31$). For all samples, the values reported for a comparable ZrO_2 specimen were used [16]. The calculated minimum shear strengths are equal to 135 and 158 MPa, for a 5 and a 10 N load, respectively. These values are much higher than the value measured (0.04 MPa) for MWCNTs [17] and those estimated from the barriers for relative axial sliding of adjacent walls, which are predicted to be negligibly small in MWCNTs [18]. The different friction and wear behaviour between ZrO_2 composites reinforced with MWCNTs (this work), SWCNTs [8] and CNFs [9] is re-

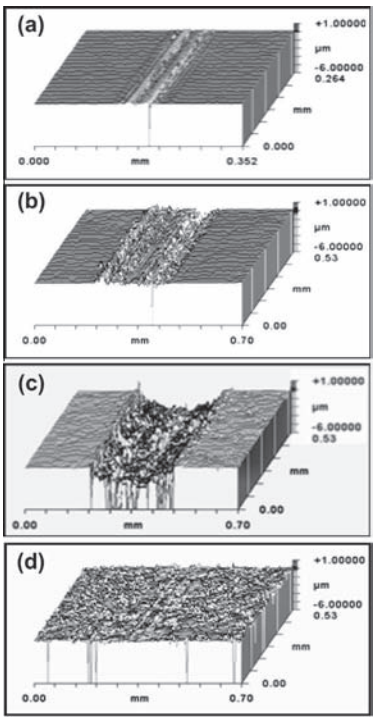

Figure 3. White-light interferometry optical images of the friction track under a 10 N load for ZrO_2 (a), S2 (b), S3 (c) and S5 (d).

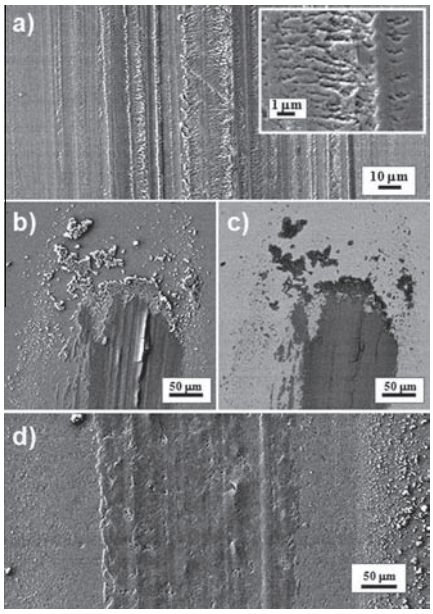

Figure 4. FESEM images of the friction tracks: ZrO_2 under a 10 N load (a), inset shows a higher-magnification image), S0.5 under a 5 N load (b and c), and S3 under a 5 N load (d).

lated to various factors including the nature of the reinforcing elements, the corresponding carbon content in the specimen, the degree of densification, matrix grain size, hardness, and fracture toughness. It appears that by using MWCNTs it is possible to lower both friction and wear when a sufficiently high content of carbon is present in the material (here 5.16 wt.% for S5). This was also shown for MWCNT–Cu composites [2] despite a decreasing relative density. Exfoliation of the MWCNTs and incorporation of the debris into a lubricating film is probable. By contrast, SWCNTs and double-walled CNTs, isolated or in bundles, require considerably higher shear stresses to be exfoliated [19] but can sustain large elastic deformations [20] and contribute to lubrication [2].

In conclusion, this work shows that MWCNT–ZrO_2 composites exhibit excellent frictional properties, with an average friction coefficient about 3.8 lower than that for ZrO_2. Exfoliation of the MWCNTs (average eight walls) due to shearing stresses and incorporation of the debris into a lubricating film over the contact area is probable. Moreover, for a higher carbon content (5.16 wt.%), wear also appears to be very low, which to the best of our knowledge has not been shown before for SWCNT– or CNF–ZrO_2 composites, but warrants further studies.

The FESEM observations were performed at TEMSCAN, the "Service Commun de Microscopie Electronique à Transmission", Université Paul Sabatier, Toulouse. The authors thank G. Chevallier for assistance with the SPS, which was performed at the Plateforme Nationale CNRS de Frittage Flash (PNF^2, Toulouse).

[1] S.R. Bakshi, D. Lahiri, A. Agarwal, Int. Mater. Rev. 55 (2010) 41.
[2] Ch. Guiderdoni, E. Pavlenko, V. Turq, A. Weibel, P. Puech, C. Estournès, A. Peigney, W. Bacsa, Ch. Laurent, Carbon 58 (2013) 185.
[3] J.-W. An, D.-H. You, D.-S. Lim, Wear 255 (2003) 677.
[4] D.-S. Lim, D.-H. You, H.-J. Choi, S.-H. Lim, H. Jang, Wear 259 (2005) 539.
[5] Z.H. Xia, J. Lou, W.A. Curtin, Scripta Mater. 58 (2008) 223.
[6] G. Yamamoto, M. Omori, K. Yokomizo, T. Hashida, K. Adachi, Mater. Sci. Eng., B 148 (2008) 265.
[7] A.K. Keshri, J. Huang, V. Singh, W.B. Choi, S. Seal, A. Agarwal, Carbon 48 (2010) 431.
[8] J.-H. Shin, S.-H. Hong, Mater. Sci. Eng., A 556 (2012) 382.
[9] P. Hvizdoš, V. Puch, A. Duszová, J. Dusza, Scripta Mater. 63 (2010) 254.
[10] Ch. Laurent, E. Flahaut, A. Peigney, Carbon 48 (2010) 2989.
[11] A. Peigney, S. Rul, F. Lefevre-Schlick, C. Laurent, J. Eur. Ceram. Soc. 27 (2007) 2183.
[12] N. Garmendia, I. Santacruz, R. Moreno, I. Obieta, J. Eur. Ceram. Soc. 29 (2009) 1939.
[13] A. Duszová, J. Dusza, K. Tomášek, G. Blugan, J. Kuebler, J. Eur. Ceram. Soc. 28 (2008) 1023.
[14] A. Duszová, J. Dusza, K. Tomášek, J. Morgiel, G. Blugan, J. Kuebler, Scripta Mater. 58 (2008) 520.
[15] J. Dusza, G. Blugan, J. Morgiel, J. Kuebler, F. Inam, T. Peijs, M.J. Reece, V. Puch, J. Eur. Ceram. Soc. 29 (2009) 3177.
[16] S. Sakaguchi, N. Murayama, Y. Kodama, F. Wakai, J. Mater. Sci. Lett. 10 (1991) 282.
[17] A. Kis, K. Jensen, S. Aloni, W. Mickelson, A. Zettl, Phys. Rev. Lett. 97 (2006) 025501.
[18] Y.E. Lozovik, A.M. Popov, Phys. Usp. 50 (2007) 749.
[19] E. Bichoutskaia, O.V. Ershova, Y.E. Lozovik, A.M. Popov, Tech. Phys. Lett. 35 (2009) 666.
[20] A.L. Aguiar, R.B. Capaz, A.G. Souza Filho, A. San Miguel, J. Phys. Chem. C. 116 (2012) 22637.